

Ultrafast Detection of ppb-Level NH₃ Gas at Room Temperature Using CuO Nanoparticles Decorated AlN-Based Surface Acoustic Wave Sensor

Na-Hyun Bak, Kedhareswara Sairam Pasupuleti, Reddeppa Maddaka, Yun-Hae Shim, Thu Thi Minh Pham, Young Heon Kim, and Moon-Deock Kim*



Cite This: <https://doi.org/10.1021/acssensors.4c01993>



Read Online

ACCESS |

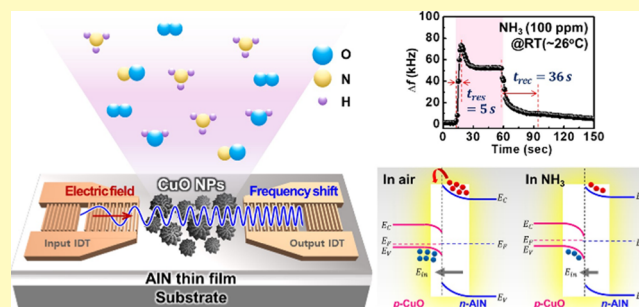
Metrics & More

Article Recommendations

Supporting Information

ABSTRACT: Rational design of heterostructure (HS)-based surface acoustic wave (SAW) smart gas sensors for efficient and accurate subppm level ammonia (NH₃) detection at room temperature (RT) is of great significance in environmental protection and human safety. This study introduced a novel HS composed of an AlN-based SAW resonator and CuO nanoparticles (NPs) as a chemical interface for NH₃ detection at RT (~26 °C). The structural, morphological, and chemical compositions were detailedly investigated, which demonstrates that the CuO/AlN HS was successfully formed via interfacial modulation. The CuO/AlN HS SAW sensor exhibited a significant positive frequency shift of 52.60 kHz in response to 100 ppm of NH₃, which is 4.8 times higher than that of the as-grown AlN SAW sensor. Additionally, the CuO/AlN HS SAW sensor exhibited ultrafast response/recovery times of 5/25 s, a remarkably low limit of detection (LOD) of 24 ppb, and excellent long-term stability and selectivity. These results are attributed to the high porosity and defect sites of CuO NPs, which enhanced charge transfer at the heterointerface, as well as decreased mass loading and conductivity effects. The CuO/AlN HS SAW sensor also demonstrated distinct frequency responses to 100 ppm of NH₃, under varying relative humidity (RH): a positive shift at low RH (5%–10%) due to increased conductivity, and a negative shift at high RH (20%–80%) due to enhanced mass loading. These NH₃ gas sensing characteristics of the CuO/AlN HS SAW sensor were validated through X-ray photoelectron spectroscopy band diagram analysis and resistive-type gas sensing measurements. These findings highlight the potential of the integrating metal oxide with nitride semiconductors for advanced SAW-based gas sensing technology in environmental and industrial applications.

KEYWORDS: CuO nanoparticles, aluminum nitride, heterojunction, SAW, NH₃ gas sensor



Ammonia (NH₃) is one of the most detrimental hazardous gases known for its colorless and pungent characteristics, primarily released from sources like animal husbandry, food processing, and industrial applications. Even at low ppm concentrations, NH₃ exposure can lead to severe health issues, including respiratory infections, pulmonary edema, and even death.^{1–6} According to the U.S Occupational Safety and Health Administration (OSHA), the maximum exposure limit of NH₃ in the workplace is set at 25 ppm for 8 h and 35 ppm for 15 min.^{4–7,51} Additionally, NH₃ is a crucial biomarker for diagnosing various diseases, such as diabetes and liver conditions, through breath analysis. It is also used in noninvasive clinical diagnoses, such as end-stage renal disease (NH₃ > 1 ppm) and hepatic encephalopathy (NH₃ > 5 ppm), where high NH₃ levels in breath indicate a metabolic disorder.^{1,3,4,7–9} Considering its risk to both health and environment, there is a crucial need for high-performance NH₃ gas sensors that operate at room temperature (RT) with

high selectivity, rapid response, and low limit of detection (LOD).

Various gas sensors, including optical, chemiresistive, and electrochemical devices, are widely available but often suffer challenges such as high operating temperatures, poor sensitivity, and long response/recovery times, requiring additional sources like light or thermal energy to boost their performance.^{1,2,5,7,10,11} Among these, surface acoustic wave (SAW) sensors based on AlN piezoelectric materials have shown promise due to their high surface acoustic velocity (~5700 m/s), selectivity, wireless operation, fast response,

Received: August 2, 2024

Revised: January 9, 2025

Accepted: January 17, 2025

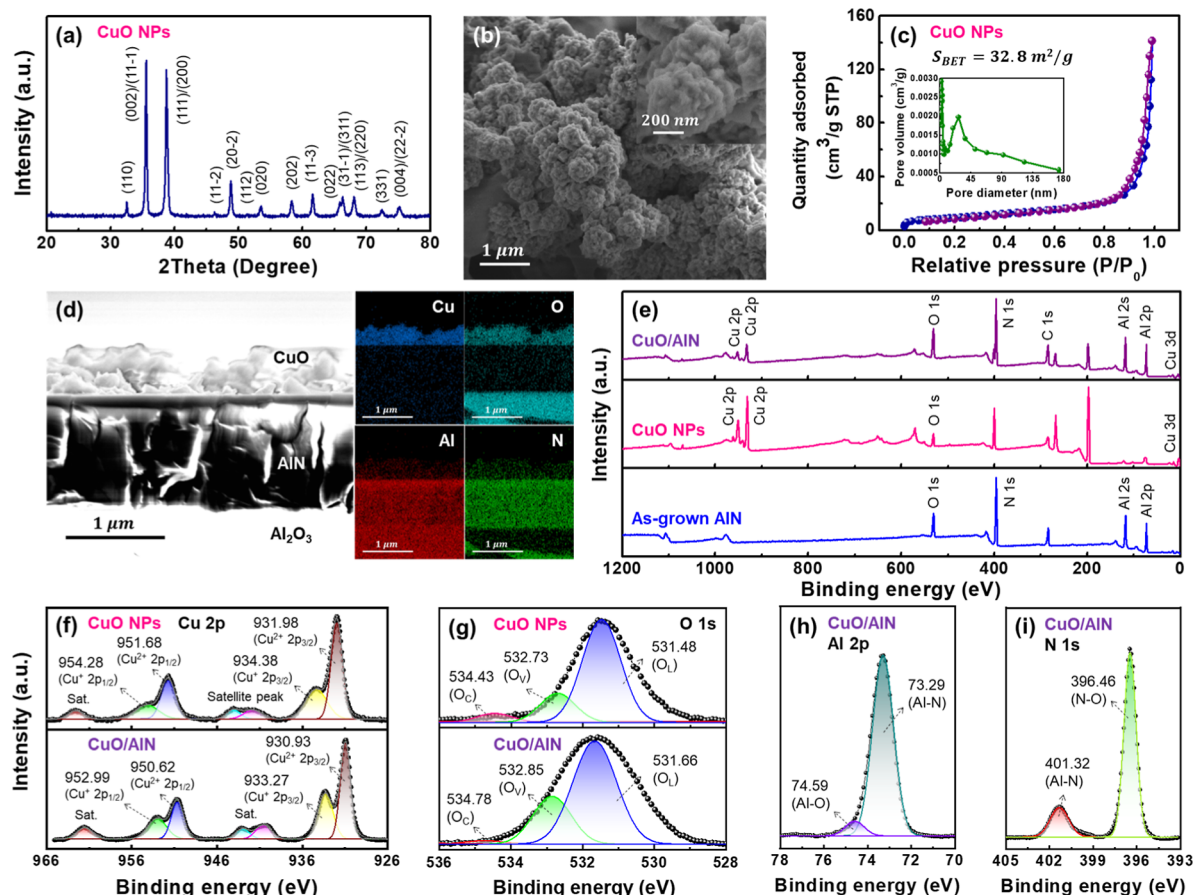


Figure 1. (a) XRD pattern, (b) SEM image of CuO NPs, (c) BET and N_2 adsorption isotherm curves of CuO NPs with pore volume (inset), (d) cross-sectional SEM image and EDX elemental mapping of CuO/AlN HS, (e) full XPS spectra of CuO/AlN HS, CuO NPs, and AlN, (f) Cu 2p and (g) O 1s spectra of CuO NPs and CuO/AlN HS, (h) Al 2p and (i) N 1s spectra of CuO/AlN HS.

stability.^{11–16} However, as-grown AlN SAW sensors struggle with low molecular sensitivity at RT due to their wide bandgap (6.2 eV).^{11,13–16} These impediments can be addressed by incorporating heterostructure (HS) with nanoparticles (NPs), 2D materials, or metal oxide semiconductors (MOS), which improve charge transport and enhance sensitivity and selectivity.^{9,11,13,17} For instance, Pd-graphene coated AlN-based HS SAW sensors demonstrated high sensitivity to H_2 gas, attributed to efficient charge transfer at the interface.¹² Thus, designing cost-effective, sensitive interfacial layer is crucial for optimizing SAW sensor performance.^{9,11–14,16,51}

Among various sensitive materials, CuO, a representative p-type MOS, has been widely studied for applications such as gas sensors, photodetectors, and energy conversion.^{5,10,18} Specifically, CuO NPs are notable for their narrow bandgap (1.3–1.6 eV), high surface area, and porous structure, which enhance their gas adsorption capacity, leading to improved sensitivity and rapid response/recovery times.^{10,19–22} Moreover, the p-type CuO combined with n-type AlN forms a heterojunction, facilitating charge separation and transport, which further improves gas sensitivity.^{13,19,20,22} Oxygen vacancies formed on the surface of CuO provide active sites for the interaction with NH_3 gas, resulting in low LOD and high selectivity.^{10,11,16,18,19,23} CuO's strong affinity for NH_3 also enables effective redox reactions, leading to a selective and stable response.^{10,18,20,22,24} Despite these advantages, few studies have explored AlN-based SAW sensors with CuO as a sensitive layer, particularly for RT NH_3 gas detection.

In this study, we developed a novel HS-based SAW sensor using single crystalline AlN thin films grown by plasma-assisted molecular beam epitaxy (PAMBE) combined with CuO NPs for NH_3 detection at RT. The CuO/AlN HS SAW sensor exhibited excellent performance, including high sensitivity, ultrafast response/recovery times, low LOD, and strong selectivity. These enhancements are attributed to improved charge transfer and reduced mass loading at the heterointerface, facilitated by the high surface area and porosity of CuO NPs. The sensor's response under varying relative humidity (RH) conditions was also evaluated, demonstrating distinct behavior that confirms its adaptability. The sensing mechanism was further analyzed through band diagram and electro-acoustic interactions, highlighting the potential of the CuO/AlN HS for efficient NH_3 detection in practical applications.

EXPERIMENTAL METHODS

The AlN thin film used in this study was grown on a sapphire substrate using PAMBE, with detailed growth conditions and parameters provided Figure S1 of the Supporting Information. Interdigital transducers (IDTs) were patterned onto the AlN film via photolithography to fabricate the SAW sensor, with detailed IDTs' design and fabrication parameters, including electrode dimensions, outlined in Figure S1c. CuO NPs were synthesized using a standard precipitation method, with synthesis details provided in Figure S1b. The synthesized CuO NPs were coated onto the delay line area of the AlN SAW resonator using the drop-casting technique (Figure S1c), forming a CuO/AlN HS. The NH_3 gas sensing system, including the setup and experimental conditions, is comprehensively described in

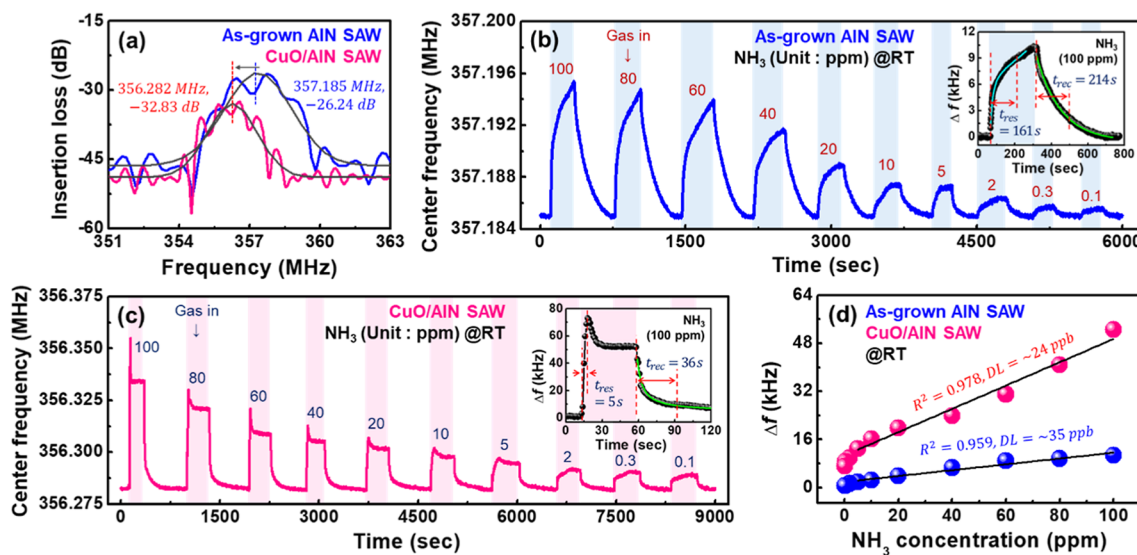


Figure 2. (a) Resonant frequency and insertion loss of as-grown AlN and CuO/AlN SAW sensors, (b) time-dependent Δf for various NH₃ concentrations (100–0.1 ppm) at RT for as-grown AlN SAW sensor, with dynamic response at 100 ppm of NH₃ (inset), (c) time-dependent Δf for various NH₃ concentrations (100–0.1 ppm) at RT for CuO/AlN HS SAW sensors, and (d) comparative summary of Δf versus NH₃ concentrations of both sensors.

Figure S1d. Additionally, the quality of the AlN thin film was evaluated using X-ray diffraction (XRD) analysis, as shown in Figure S2.

RESULTS AND DISCUSSION

Figure 1a depicts the XRD patterns of the synthesized CuO NPs, with peaks corresponding to various crystal planes, confirming the successful synthesis of monoclinic-phase CuO (JCPDS card no. 48-1548).^{9,10,19,20,25} The scanning electron microscopy (SEM) image in Figure 1b reveals densely packed, spherical CuO NPs with a porous structure (inset). The UV-visible spectra and Tauc plot for CuO NPs, presented in Figure S3, confirm an indirect bandgap of 1.44 eV.²⁴ The sharp absorption peak below 732 nm in the UV-vis spectra indicates the high crystallinity of CuO NPs, consistent with the XRD results. Figure 1c displays the Brunauer–Emmett–Teller (BET) N₂ adsorption/desorption isotherms, showing type-IV behavior with a mesoporous structure (inset: pore size distribution).²² The BET surface area of CuO NPs was found to be 32.62 m²/g with an average pore size of 32.6 nm, which indicates enhanced gas adsorption on the sensing surface.^{9,19,22,26} Figure 1d displays the cross-sectional SEM image and energy dispersive X-ray spectroscopy (EDX) mapping and SEM image of the CuO/AlN HS. The mapping confirms coating of Cu, O, Al, and N elements, with the CuO NPs layer having an average thickness of 320 ± 20 nm on the AlN SAW device.^{10,20,25} The chemical bond interactions, charge transfer, and electron states of the CuO NPs, AlN, and CuO/AlN HS samples were investigated using wide-survey scan X-ray photoelectron spectroscopy (XPS) spectra (Figure 1e). In comparison to CuO NPs and the as-grown AlN, the CuO/AlN HS XPS spectra revealed the presence of key elements (Al, N, Cu, O, and C) along with CuO NPs satellite peaks, confirming successful CuO coating on the AlN surface. The high-resolution Cu 2p XPS peak of the CuO/AlN HS (Figure 1f) resolved seven peaks, with dominant bands at 933.27, 930.93 eV (Cu 2p_{3/2}), and 952.99, 950.62 eV (Cu 2p_{1/2}), exhibiting a spin-energy separation of 19.70 eV, indicating the presence of Cu(I), and Cu(II) oxidation

state.^{18,20,27,28} Four satellite peaks (961.57, 934.28, 942.99, and 940.56 eV) indicate the paramagnetic state of Cu²⁺ ions based on the configuration of Cu atom.^{20,22,25–27} A significant shift in core binding energies between CuO NPs and CuO/AlN HS suggests enhanced charge transfer at the interface, improving sensor sensitivity and gas kinetics at RT.^{16,20,22,23} The O 1s XPS spectra of CuO NPs (Figure 1g) were deconvoluted into three peaks at 534.43, 532.73, and 531.48 eV, corresponding to chemisorbed oxygen (O_C), oxygen vacancies (O_V), and lattice oxygen (O_L) from surface-adsorbed H₂O molecules (Cu–OH), respectively.^{18,29,31} The CuO/AlN HS sample showed similar peaks at 534.78, 532.85, and 531.66 eV, with an increase in oxygen vacancies, enhancing O₂ adsorption.^{9,16,20,23,25} The high-resolution XPS Al 2p spectrum (Figure 1h) showed peaks at 73.29 and 74.59 eV, corresponding to Al–N and Al–O bonds.¹⁶ The N 1s spectrum (Figure 1i) exhibited peaks at 401.32 and 396.46 eV, indicating Al–N and N–O bonds, confirming the epitaxial growth of AlN.¹⁶ Overall, the XPS analysis confirms the formation of the CuO/AlN HS with enhanced oxygen vacancies and chemical interactions, which is crucial for improved gas sensing performance.

Figure 2a shows the comparative resonating frequency characteristics of the as-grown AlN SAW sensor and the CuO/AlN HS SAW sensor. The CuO NPs layer on the delay line caused a negative shift in the center frequency from 357.185 to 356.282 MHz and a decrease in insertion loss from -26.24 to -32.83 dB. These changes were attributed to the mass loading effect of the CuO NPs coating, which affected the SAW propagation.^{12,14,15,30,51} Figure 2b,c show the dynamic transient response and recovery gas sensing characteristics of both SAW sensors to various NH₃ concentrations ranging from 0.1 to 100 ppm. Both SAW sensors exhibited a positive frequency shift (Δf) to NH₃ with a linear increment relative NH₃ concentration. Compared to the as-grown AlN SAW sensor (10.79 kHz), the CuO/AlN HS SAW sensor (52.60 kHz) showed 4.8 times higher Δf to 100 ppm of NH₃, as shown in Figure 2d. The theoretical LODs of the as-grown AlN SAW and the CuO/AlN HS SAW sensors were calculated

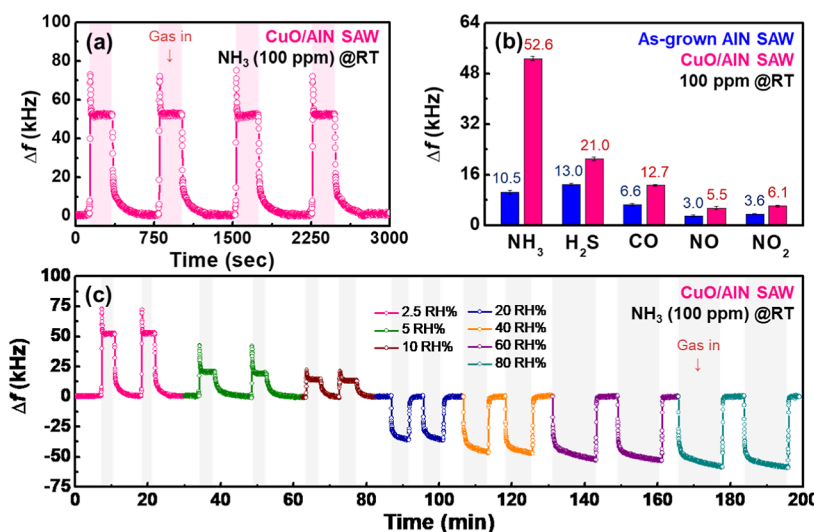


Figure 3. (a) Repeatability of CuO/AlN HS SAW sensor at 100 ppm of NH₃, (b) selectivity comparison of as-grown AlN and CuO/AlN HS SAW sensors to various gases at 100 ppm, and (c) dynamic Δf under varying RH from 2.5% to 80% at 100 ppm of NH₃ at RT for CuO/AlN HS SAW sensor.

to be 35 and 24 ppb, respectively, with detailed calculation steps and the LOD equation, provided in Figure S4.^{4,8,32,33} The dynamic response to 100 ppm of NH₃ of each sensor is shown in the inset of Figure 2b,c, where the as-grown AlN SAW sensor exhibited response/recovery times of 161/214 s, while the CuO/AlN HS SAW sensor demonstrated much faster times of 5/36 s. Detailed analysis of response and recovery times for various NH₃ concentrations is provided in Figure S5.^{31,38,39–42,45}

Factors such as cycling repeatability, long-term stability, and reliable selectivity are crucial for sensors operating at RT in practical applications. Figure 3a demonstrates the cycling stability and repeatability of the CuO/AlN HS SAW sensor under 100 ppm of NH₃ for four cycles, showing a constant Δf and consistent response and recovery times. The long-term stability test (Figure S6) showed only a 1.23% loss in Δf over six months, confirming the sensor's durability. Figure 3b shows the superior selectivity and sensitivity of the CuO/AlN HS SAW sensor to NH₃ compared to other test gases. Table S1 provides further comparison with published data, highlighting its promising performance at RT. This enhanced selectivity can be attributed to interface engineering and the unique properties of CuO NPs, which possess multiple oxidation states and a d⁹ electronic configuration.^{19,33,38,39,40} These properties allow CuO to effectively retain cations with filled outer orbitals and generate free electrons upon contact with reducing agents like NH₃.^{19,21}

Additionally, the effect of RH on the CuO/AlN HS SAW sensor performance was studied by varying RH from ~0% to 80% under 100 ppm of NH₃ at RT (~26 °C), as shown in Figure 3c. Under low RH conditions (0%–10%), the CuO/AlN HS SAW sensor exhibited a positive shift, but the magnitude of the shift gradually decreased as RH increased. Conversely, under high RH conditions (20%–80%), the CuO/AlN HS SAW sensor showed a negative Δf , with the magnitude increasing as RH levels rose. The humidity sensing mechanism of the CuO/AlN HS SAW sensor will be explained using the Grotthuss mechanism in the following section.^{5,13,14,17,32,51} Figure S7 provides a detailed summary of Δf and response/recovery times at different RH levels. These

data confirm that the CuO/AlN HS SAW sensor effectively detects NH₃ gas across varying humidity levels, demonstrating its robustness in practical applications.

Gas Sensing Mechanism. The Δf of both SAW sensors in response to NH₃ is determined by modulations in acoustic wave propagation, influenced by gas molecules adsorption on the sensing layer, as described by eq 1.^{11,32,34,35,41,42} In this equation, the first and third terms correspond to changes in mass and electroacoustic (conductivity) loading effects, causing a negative Δf , while the second term indicates the elastic loading effect, causing a positive Δf .^{9,11,32,36,51}

$$\frac{\Delta f}{f_0} = \frac{\Delta v}{v_0} \\ = -C_m f_0 \Delta(\rho_s) + C_f f_0 h \Delta \left\{ \frac{4\mu}{v_0^2} \left(\frac{\mu+1}{\mu+2\lambda} \right) \right\} \\ - \frac{K^2}{2} \Delta \left\{ \frac{1}{1 + \left(\frac{v_0 C_s}{\sigma_s} \right)^2} \right\} \quad (1)$$

In the first, the as-grown AlN SAW sensor exhibited a positive Δf in response to NH₃, primarily due to the increased elastic loading effect.^{9,11,51} When exposed to NH₃, gas molecules adsorbed onto the sensor surface and interact with surface defects and functional groups. These interactions form interfacial hydrogen bonds via weak van der Waals forces, affecting the local bonding environment.^{11,36,37,45} The adsorbed NH₃ molecules can donate their lone pairs of electrons to the surface atoms of AlN, leading to the formation of surface complexes and causing changes in the local electric field or polarization state, which in turn can affect the mechanical properties of the AlN surface, such as stiffening or softening.^{9,18,33} The effective interaction between NH₃ molecules and AlN induces stress on the AlN surface due to the force exerted by the adsorbed NH₃ molecules, consistent with reported literature.^{9,46–48} Furthermore, AlN is a typical n-type semiconductor, which increases electrical conductivity upon contact with reducing gases like NH₃, leading to a

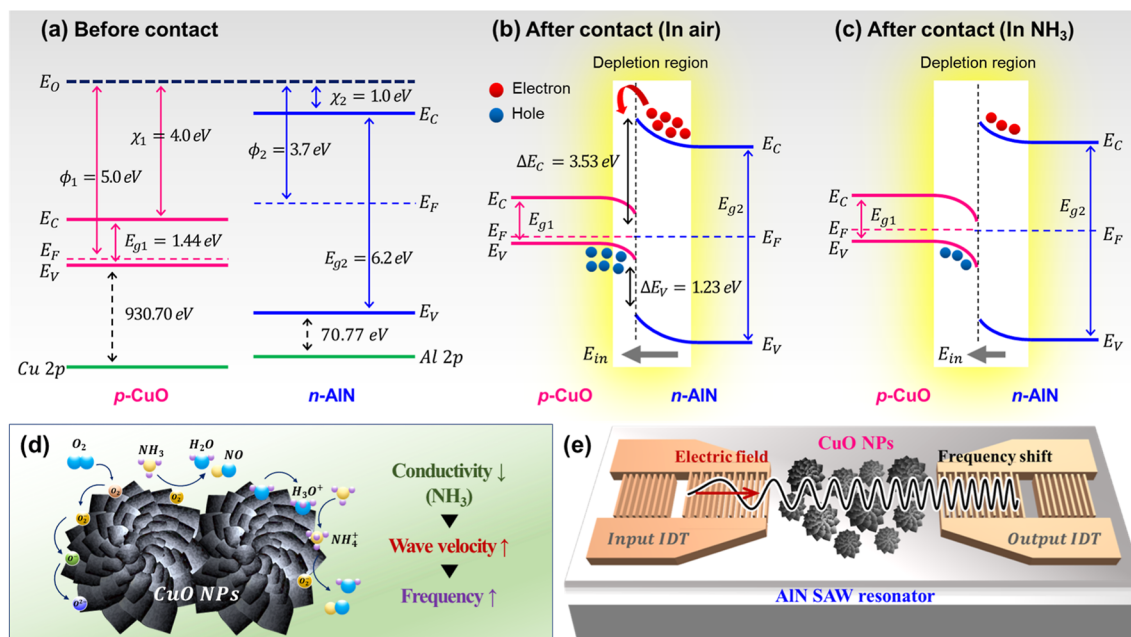


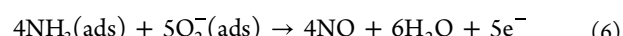
Figure 4. (a) Energy band diagram of the CuO/AlN HS SAW sensor before contact, (b) energy band diagram after contact (in air), (c) energy band diagram after contact (in NH_3), (d) chemical reactions between NH_3 and CuO NPs, and (e) SAW gas sensing mechanism.

negative Δf .^{9,33,51} However, the NH_3 sensing results of the as-grown AlN SAW sensor in this work showed a positive Δf , clearly suggesting that this response is mainly due to the elastic loading effect.^{9,14}

The CuO/AlN HS SAW sensor exhibited a positive Δf in response to NH_3 . This result is primarily due to variations in both the conductivity and mass of the CuO/AlN HS interface.^{9,11,14,51} It is noteworthy that NH_3 molecules have a low molecular density (17.03 g/mol), much lower than that of other interfering gases ($\text{NO}_2 > \text{NO} > \text{H}_2\text{S} > \text{CO} > \text{NH}_3$). Thus, the lower mass loading effect on the SAW sensor surface may also result in higher acoustic wave propagation, causing a positive Δf .^{9,33,43} Additionally, to confirm the role of CuO in the sensing process, we measured a resistive-type p-CuO NPs sensor under NH_3 gas. As shown in Figure S8a, its resistance increases under NH_3 exposure, indicating a decrease in conductivity consistent with the response of the CuO/AlN HS SAW sensor. The resistive-type sensor exhibited an approximately 33.3% response and 9.3/56 min response/recovery times at 100 ppm of NH_3 (Figure S8b,c), confirming that CuO undergoes reduced conductivity when exposed to NH_3 , thereby contributing to the SAW sensor's positive frequency shift.

To investigate charge transfer at the CuO/AlN HS interface, we performed an XPS-based band analysis, with detailed XPS data and band offset calculations using the Kraut method provided in Figure S9a–c. Based on this XPS analysis, we calculated the initial band alignment of p-type CuO and intrinsic n-type AlN before forming the HS, as shown in Figure 4a. Upon forming the HS, electron transfer from n-AlN to p-CuO occurs due to the work function difference until thermal equilibrium is achieved. This electron flow results in significant downward band bending in p-CuO and upward band bending in n-AlN.^{5,20,33,49} Under ambient air conditions, oxygen molecules adsorb onto the CuO/AlN HS surface, capturing free electrons from the interface and forming oxygen ions (O_2^-), as shown in (eqs 2–5). This creates a depletion region and establishes a strong internal electric field at the interface, as

visualized in Figure 4b.^{5,18,21,22,50} This electric field is crucial as it facilitates rapid interaction with NH_3 , thereby accelerating reaction kinetics and reducing response time.⁵¹ When exposed to NH_3 , the gas molecules physically adsorb onto the HS interface and react with the preadsorbed oxygen ions, releasing electrons back into the conduction band of CuO, as per eq 6. These electrons recombine with holes in CuO, significantly reducing the charge carrier density at the HS interface. This reduction in carriers weakens the electric field and broadens the depletion layer (Figure 4c), thereby lowering the conductivity of the CuO layer (equivalently, raising the overall sensor resistance, Figure 4d).^{5,23,52} Although the electron density of AlN may slightly increase, its intrinsic properties limit any substantial change to the sensor conductivity.⁵³ Consequently, the decrease in conductivity at the CuO/AlN interface facilitates faster SAW propagation, leading to a notable positive Δf , as depicted in Figure 4e.^{5,6,16,21–23,54}



At low RH levels (5%–10%), the CuO/AlN HS SAW sensor exhibited a positive Δf , explained by the Grotthuss mechanism (eq 7), where H_2O molecules dissociate into H^+ and OH^- ions at the HS interface.^{5,33,54} This dissociation increases the conductivity, which hinders SAW propagation and leads to a decreasing Δf as RH increases.^{5,9,17,33,51} In contrast, at high RH levels (20–80 RH %), the physical adsorption of H_2O molecules forms hydronium ions (H_3O^+) and multilayer adsorption, causing a negative Δf due to increased mass loading.^{5,17,33,43,44,54} As RH rises, a large quantity of H_3O^+ is generated via proton hopping, which attracts more NH_3 gas

molecules.^{5,33,43,44} The adsorbed NH₃ molecules interact with H₃O⁺ and H₂O, potentially forming NH₄⁺ radicals. This further increases mass loading, enhancing the negative Δf . Additionally, the generation of NH₄⁺ radicals and oxidation reactions with O₂⁻ ions at higher RH levels reduce the sensor's conductivity.^{9,11,13,14,51,55} At higher RH, the thicker H₂O layer slows charge transfer, resulting in longer response times.^{5,14,51} However, when RH decreases, the desorption of H₂O and NH₃ leads to rapid recovery, as shown in Figure S7b.^{9,17,S1,S4,S6,S7}



In summary, the CuO/AlN HS SAW sensor's ultrafast, highly sensitive, and selective NH₃ detection at RT can be attributed to several factors: (i) the high surface acoustic velocity of AlN (~5700 m/s) enabling rapid response/recovery times and stability; (ii) the high porosity and surface area of CuO NPs providing abundant active sites for gas adsorption; (iii) effective charge carrier control at the HS interface enhancing sensitivity and response; and (iv) oxygen vacancies and defect sites boosting NH₃ adsorption. These combined effects lead to the sensor's excellent performance.

CONCLUSION

A novel CuO/AlN HS-based SAW sensor was successfully fabricated for NH₃ detection at RT. Material characterization and XPS band analysis confirmed the HS formation between CuO and AlN. The CuO/AlN HS SAW sensor exhibited ultrafast response/recovery times of 5/25 s and a significant positive Δf of 52.60 kHz to 100 ppm of NH₃ at RT. It also demonstrated a low LOD of 24 ppb, excellent repeatability, and a reliable long-term stability. The superior sensing performance of the CuO/AlN HS SAW sensor is primarily due to its reduced conductivity and decreased mass loading effect. The CuO/AlN HS interface facilitates efficient charge transfer between NH₃ molecules and adsorbed O₂ ions, contributing to high selectivity and stability. Furthermore, the porosity, large surface area, and defect sites of CuO NPs enable superior O₂ adsorption. In addition, the CuO/AlN HS SAW sensor exhibited distinct responses to NH₃ (100 ppm) under different RH conditions. At low RH (5%–10%), a positive Δf was observed, primarily due to increased conductivity from H₂O dissociation. At higher RH levels (20%–80%), a negative Δf was caused by mass loading from multilayer H₂O adsorption. These results demonstrate that the CuO/AlN HS SAW sensor is highly adaptable to varying environmental conditions while maintaining excellent sensitivity and selectivity for NH₃. This work highlights a promising AlN-based SAW gas sensor platform with potential applicability for detecting various toxic gases. Moreover, we expect that optimization of the SAW IDT structure and integration of diverse sensing materials may further enhance the overall performance of the CuO/AlN HS SAW sensor.

ASSOCIATED CONTENT

Supporting Information

The Supporting Information is available free of charge at <https://pubs.acs.org/doi/10.1021/acssensors.4c01993>.

Supplementary figures detailing the material synthesis, device fabrication process, and gas sensing system, including raw measurement results. Additional spectral

data and detailed analysis supporting the main findings are also provided ([PDF](#))

AUTHOR INFORMATION

Corresponding Author

Moon-Deock Kim – Department of Physics, Chungnam National University, Daejeon 34134, Republic of Korea; Department of Physics and Institute of Quantum Systems (IQS), Chungnam National University, Daejeon 34134, Republic of Korea; [orcid.org/0000-0002-7622-8488](#); Phone: +82 42 821 5452; Email: mdkim@cnu.ac.kr; Fax: +82 42 822 8011

Authors

Na-Hyun Bak – Department of Physics, Chungnam National University, Daejeon 34134, Republic of Korea; [orcid.org/0000-0002-1321-1662](#)

Kedhareswara Sairam Pasupuleti – Department of Physics and Institute of Quantum Systems (IQS), Chungnam National University, Daejeon 34134, Republic of Korea; [orcid.org/0000-0002-3508-6890](#)

Reddeppa Maddaka – Department of Electrical Engineering and Computer Science, University of Michigan, Ann Arbor, Michigan 48109, United States; [orcid.org/0009-0007-4991-7177](#)

Yun-Hae Shim – Department of Physics, Chungnam National University, Daejeon 34134, Republic of Korea; [orcid.org/0009-0009-7052-2166](#)

Thu Thi Minh Pham – Graduate School of Analytical Science and Technology (GRAST), Chungnam National University, Daejeon 34134, Republic of Korea; [orcid.org/0009-0008-8260-7151](#)

Young Heon Kim – Graduate School of Analytical Science and Technology (GRAST), Chungnam National University, Daejeon 34134, Republic of Korea; [orcid.org/0000-0001-9944-5859](#)

Complete contact information is available at:

<https://pubs.acs.org/10.1021/acssensors.4c01993>

Notes

The authors declare no competing financial interest.

ACKNOWLEDGMENTS

This work was supported by BK21 FOUR Program by Chungnam National University Research grant, 2022 and Basic Science Research Program through the National Research Foundation of Korea (NRF) funded by the Ministry of Education (RS-2020-NR049597).

REFERENCES

- (1) Chen, Y.; Fu, H.; Bai, Y.; Yang, X.; Xiong, S.; Han, D.; An, X. Room-temperature NH₃-sensor: SnO₂@PANI core-shell hollow spheres. *Sens. Actuators, B* **2024**, *412*, 135784.
- (2) Goswami, P.; Gupta, G. Recent progress of flexible NO₂ and NH₃ gas sensors based on transition metal dichalcogenides for room temperature sensing. *Mater. Today Chem.* **2022**, *23*, 100726.
- (3) Lu, X.; Qu, Y.; Zhang, F.; Ding, Z.; Zheng, H.; Lei, Y.; Liu, S.; Li, S. A sensitive NH₃ chemiresistive sensor with wide detection range: Employing a MOF-derived mesoporous carbon composite with polyaniline. *Sens. Actuators, B* **2024**, *416*, 135938.
- (4) Tanaka, K.; Cheng, G.; Nakamura, T.; Hiraoka, K.; Tabata, H.; Kubo, O.; Komatsu, N.; Katayama, M. NH₃ Gas Sensors Based on Single-Walled Carbon Nanotubes Interlocked with Metal-Tethered

- Tetragonal Nanobrackets. *ACS Appl. Nano Mater.* **2024**, *7* (11), 13417–13425.
- (5) Zhu, X.; Li, J.; Chang, X.; Gao, W.; Chen, X.; Niu, S.; Sun, S. Room temperature gas sensors for NH₃ detection based on SnO₂ films and lamellar-structured Ti₃C₂Tx MXene heterojunction nanocomposites. *Appl. Surf. Sci.* **2024**, *660*, 159976.
- (6) Ravikumar, T.; Sivaperuman, K. Fabrication of bare and cobalt-doped ZnFe₂O₄ thin film as NH₃ gas sensor with enhanced response through UV-light illumination. *Mater. Today Chem.* **2024**, *38*, 102049.
- (7) Mirzaei, A.; Alizadeh, M.; Ansari, H. R.; Moayedi, M.; Kordrostami, Z.; Safaeian, H.; Lee, M. H.; Kim, T.; Kim, J.; Kim, H. W.; et al. Resistive gas sensors for the detection of NH₃ gas based on 2D WS₂, WSe₂, MoS₂, and MoSe₂: A review. *Nanotechnology* **2024**, *35*, 332002.
- (8) Moshayedi, A. J.; Sohail Khan, A.; Hu, J.; Nawaz, A.; Zhu, J. E-nose-driven advancements in ammonia gas detection: a comprehensive review from traditional to cutting-edge systems in indoor to outdoor agriculture. *Sustainability* **2023**, *15* (15), 11601.
- (9) Xu, X.; Zu, X.; Ao, D.; Yu, J.; Xiang, X.; Xie, W.; Tang, Y.; Li, S.; Fu, Y. NH₃-Sensing Mechanism Using Surface Acoustic Wave Sensor with AlO(OH) Film. *Nanomaterials* **2019**, *9* (12), 1732.
- (10) Khan, H. U.; Tariq, M.; Shah, M.; Iqbal, M.; Jan, M. T. Inquest of highly sensitive, selective and stable ammonia (NH₃) gas sensor: Structural, morphological and gas sensing properties of polyvinylpyrrolidone (PVP)/CuO nanocomposite. *Synth. Met.* **2020**, *268*, 116482.
- (11) Xiong, S.; Liu, X.; Zhou, J.; Liu, Y.; Shen, Y.; Yin, X.; Wu, J.; Tao, R.; Fu, Y.; Duan, H. Stability studies of ZnO and AlN thin film acoustic wave devices in acid and alkali harsh environments. *RSC Adv.* **2020**, *10* (33), 19178–19184.
- (12) Ha, N. H.; Nam, N. H.; Dung, D. D.; Phuong, N. H.; Thach, P. D.; Hong, H. S. Hydrogen Gas Sensing Using Palladium-Graphene Nanocomposite Material Based on Surface Acoustic Wave. *J. Nanomater.* **2017**, *2017* (1), 1–6.
- (13) Le, X.; Wang, X.; Pang, J.; Liu, Y.; Fang, B.; Xu, Z.; Gao, C.; Xu, Y.; Xie, J. A high performance humidity sensor based on surface acoustic wave and graphene oxide on AlN/Si layered structure. *Sens. Actuators, B* **2018**, *255*, 2454–2461.
- (14) Pang, J.; Dong, H.; Pang, K.; Le, X.; Xu, Z.; Gao, C.; Xie, J. Selective Detection of CO₂ and H₂O Dual Analytes Through Decoupling Surface Density and Shear Modulus Based on Single SAW Resonator. *IEEE Electron Device Lett.* **2022**, *43* (3), 450–453.
- (15) Streque, J.; Camus, J.; Laroche, T.; Hage-Ali, S.; M'Jahed, H.; Rammal, M.; Aubert, T.; Djouadi, M. A.; Ballandras, S.; Elmazria, O. Design and Characterization of High-Q SAW Resonators Based on the AlN/Sapphire Structure Intended for High-Temperature Wireless Sensor Applications. *IEEE Sensor. J.* **2020**, *20* (13), 6985–6991.
- (16) Hermawan, A.; Asakura, Y.; Yin, S. Morphology control of aluminum nitride (AlN) for a novel high-temperature hydrogen sensor. *Int. J. Miner. Metall. Mater.* **2020**, *27* (11), 1560–1567.
- (17) Li, R.; Fan, Y.; Ma, Z.; Zhang, D.; Liu, Y.; Xu, J. Controllable preparation of ultrathin MXene nanosheets and their excellent QCM humidity sensing properties enhanced by fluoride doping. *Microchim. Acta* **2021**, *188*, 81–11.
- (18) Tsymbalenko, O.; Lee, S.; Lee, Y.-M.; Nam, Y.-S.; Kim, B. C.; Kim, J. Y.; Lee, K.-B. High-sensitivity NH₃ gas sensor using pristine graphene doped with CuO nanoparticles. *Microchim. Acta* **2023**, *190* (4), 134.
- (19) Sakthivel, B.; Manjakkal, L.; Nammalvar, G. High Performance CuO Nanorectangles-Based Room Temperature Flexible NH₃ Sensor. *IEEE Sensor. J.* **2017**, *17* (20), 6529–6536.
- (20) Seekaew, Y.; Kamlue, S.; Wongchoosuk, C. Room-Temperature Ammonia Gas Sensor Based on Ti₃C₂Tx MXene/Graphene Oxide/CuO/ZnO Nanocomposite. *ACS Appl. Nano Mater.* **2023**, *6* (10), 9008–9020.
- (21) Shao, F.; Hernández-Ramírez, F.; Prades, J. D.; Fàbrega, C.; Andreu, T.; Morante, J. R. Copper (II) oxide nanowires for p-type conductometric NH₃ sensing. *Appl. Surf. Sci.* **2014**, *311*, 177–181.
- (22) Liu, M.; Ding, Y.; Lu, Z.; Song, P.; Wang, Q. Layered Ti₃C₂Tx MXene/CuO spindles composites for NH₃ detection at room-temperature. *J. Alloys Compd.* **2023**, *938*, 168563.
- (23) Zang, C.; Ma, K.; Yano, Y.; Li, S.; Yamahara, H.; Seki, M.; Iizuka, T.; Tabata, H. SnO₂–CuO Heterostructured Nanofibers for Enhanced NH₃-Gas-Sensing Performance and Potential Application in Breath Analysis. *IEEE Sensor. J.* **2023**, *23* (16), 17925–17931.
- (24) Abdelbasir, S. M.; Rayan, D. A.; Ismail, M. M. Synthesis of Cu and CuO nanoparticles from e-waste and evaluation of their antibacterial and photocatalytic properties. *Environ. Sci. Pollut. Res.* **2023**, *30* (38), 89690–89704.
- (25) Luo, H.; Shi, J.; Liu, C.; Chen, X.; Lv, W.; Zhou, Y.; Zeng, M.; Yang, J.; Wei, H.; Zhou, Z.; et al. Design of p–p heterojunctions based on CuO decorated WS₂ nanosheets for sensitive NH₃ gas sensing at room temperature. *Nanotechnology* **2021**, *32* (44), 445502.
- (26) Rajak, R.; Saraf, M.; Kumar, P.; Natarajan, K.; Mobin, S. M. Construction of a Cu-based metal–organic framework by employing a mixed-ligand strategy and its facile conversion into nanofibrous CuO for electrochemical energy storage applications. *Inorg. Chem.* **2021**, *60* (22), 16986–16995.
- (27) Liu, Y.; Cao, X.; Jiang, D.; Jia, D.; Liu, J. Hierarchical CuO nanorod arrays in situ generated on three-dimensional copper foam via cyclic voltammetry oxidation for high-performance supercapacitors. *J. Mater. Chem. A* **2018**, *6* (22), 10474–10483.
- (28) Xu, H.; Wang, D.; Ma, J.; Zhang, T.; Lu, X.; Chen, Z. A superior active and stable spinel sulfide for catalytic peroxymonosulfate oxidation of bisphenol S. *Appl. Catal., B* **2018**, *238*, 557–567.
- (29) Nathan, M. G. T.; Boby, S. J. M.; Mahesh, R.; Basu, P.; Joseph, S.; Sagayaraj, P.; Joseph, S. One-pot hydrothermal preparation of Cu₂O-CuO/rGO nanocomposites with enhanced electrochemical performance for supercapacitor applications. *Appl. Surf. Sci.* **2018**, *449*, 474–484.
- (30) Tomar, A. K.; Singh, G.; Sharma, R. K. Fabrication of a Mo-doped strontium cobaltite perovskite hybrid supercapacitor cell with high energy density and excellent cycling life. *ChemSusChem* **2018**, *11* (23), 4123–4130.
- (31) Xiong, S.; Zhou, J.; Wu, J.; Li, H.; Zhao, W.; He, C.; Liu, Y.; Chen, Y.; Fu, Y.; Duan, H. High performance acoustic wave nitrogen dioxide sensor with ultraviolet activated 3D porous architecture of Ag-decorated reduced graphene oxide and polypyrrole aerogel. *ACS Appl. Mater. Interfaces* **2021**, *13* (35), 42094–42103.
- (32) Pasupuleti, K. S.; Reddeppa, M.; Nam, D.-J.; Bak, N.-H.; Peta, K. R.; Cho, H. D.; Kim, S.-G.; Kim, M.-D. Boosting of NO₂ gas sensing performances using GO-PEDOT: PSS nanocomposite chemical interface coated on langasite-based surface acoustic wave sensor. *Sens. Actuators, B* **2021**, *344*, 130267.
- (33) Pasupuleti, K. S.; Reddeppa, M.; Chougule, S.; Bak, N.-h.; Nam, D.-J.; Jung, N.; Cho, H. D.; Kim, S.-G.; Kim, M.-D. High performance langasite based SAW NO₂ gas sensor using 2D g-C₃N₄@ TiO₂ hybrid nanocomposite. *J. Hazard. Mater.* **2022**, *427*, 128174.
- (34) Ponzoni, A. A statistical analysis of response and recovery times: the case of ethanol chemiresistors based on pure SnO₂. *Sensors* **2022**, *22* (17), 6346.
- (35) Yaqoob, U.; Younis, M. I. Chemical gas sensors: Recent developments, challenges, and the potential of machine learning A review. *Sensors* **2021**, *21* (8), 2877.
- (36) Saruhan, B.; Lontio Fomekong, R.; Nahirniak, S. Influences of semiconductor metal oxide properties on gas sensing characteristics. *Frontiers in Sens.* **2021**, *2*, 657931.
- (37) Jiang, Y.; Li, W.; Du, F.; Sokolovskij, R.; Zhang, Y.; Shi, S.; Huang, W.; Wang, Q.; Yu, H.; Wang, Z. A comprehensive review of gallium nitride (GaN)-based gas sensors and their dynamic responses. *J. Mater. Chem. C* **2023**, *11* (30), 10121–10148.
- (38) Wawrzyniak, J. Advancements in improving selectivity of metal oxide semiconductor gas sensors opening new perspectives for their application in food industry. *Sensors* **2023**, *23* (23), 9548.
- (39) Tang, Y.; Wu, W.; Wang, B.; Dai, X.; Xie, W.; Yang, Y.; Zhang, R.; Shi, X.; Zhu, H.; Luo, J.; et al. H₂S gas sensing performance and mechanisms using CuO-Al₂O₃ composite films based on both surface

- acoustic wave and chemiresistor techniques. *Sens. Actuators, B* **2020**, 325, 128742.
- (40) Martínez-Ahumada, E.; Díaz-Ramírez, M. L.; Velásquez-Hernández, M. d. J.; Jancik, V.; Ibarra, I. A. Capture of toxic gases in MOFs: SO₂, H₂S, NH₃ and NO x. *Chem. Sci.* **2021**, 12 (20), 6772–6799.
- (41) Cheeke, J.; Wang, Z. Acoustic wave gas sensors. *Sens. Actuators, B* **1999**, 59 (2–3), 146–153.
- (42) Pasupuleti, K. S.; Thomas, A. M.; Vidyasagar, D.; Rao, V. N.; Yoon, S.-G.; Kim, Y.-H.; Kim, S.-G.; Kim, M.-D. ZnO@ Ti3C2T x MXene Hybrid Composite-Based Schottky-Barrier-Coated SAW Sensor for Effective Detection of Sub-ppb-Level NH₃ at Room Temperature under UV Illumination. *ACS Mater. Lett.* **2023**, 5 (10), 2739–2746.
- (43) Pasupuleti, K. S.; Ghosh, S.; Jayababu, N.; Kang, C.-J.; Cho, H. D.; Kim, S.-G.; Kim, M.-D. Boron doped g-C₃N₄ quantum dots based highly sensitive surface acoustic wave NO₂ sensor with faster gas kinetics under UV light illumination. *Sens. Actuators, B* **2023**, 378, 133140.
- (44) Pasupuleti, K. S.; Nam, D.-J.; Bak, N.-h.; Reddeppa, M.; Oh, J.-E.; Kim, S.-G.; Cho, H. D.; Kim, M.-D. Highly sensitive gC₃N₄ nanosheets as a potential candidate for the effective detection of NO₂ gas via langasite-based surface acoustic wave gas sensor. *J. Mater. Chem. C* **2021**, 10 (1), 160–170.
- (45) Li, Y.; Zhang, C.; Luo, X.; Liang, Y.; Wuu, D.-S.; Tin, C.-C.; Lu, X.; He, K.; Wan, L.; Feng, Z. C. Surface, structural and optical properties of AlN thin films grown on different face sapphire substrates by metalorganic chemical vapor deposition. *Appl. Surf. Sci.* **2018**, 458, 972–977.
- (46) Liu, D.; Robertson, J. Oxygen vacancy levels and interfaces of Al₂O₃. *Microelectron. Eng.* **2009**, 86 (7–9), 1668–1671.
- (47) Zeng, J.; Wu, G.; Shi, W.; Chen, S. First-Principles Study on Properties of the Native Defects in Al₂O₃ (110) Surface. *Protect. Met. Phys. Chem. Surface* **2019**, S5, 631–636.
- (48) Schilirò, E.; Fiorenza, P.; Bongiorno, C.; Spinella, C.; Di Franco, S.; Greco, G.; Lo Nigro, R.; Roccaforte, F. Correlating electron trapping and structural defects in Al₂O₃ thin films deposited by plasma enhanced atomic layer deposition. *AIP Adv.* **2020**, 10 (12), 125017.
- (49) Kraut, E.; Grant, R.; Waldrop, J.; Kowalczyk, S. Precise determination of the valence-band edge in x-ray photoemission spectra: application to measurement of semiconductor interface potentials. *Phys. Rev. Lett.* **1980**, 44 (24), 1620.
- (50) Pasupuleti, K. S.; Chougule, S. S.; Vidyasagar, D.; Bak, N.-h.; Jung, N.; Kim, Y.-H.; Lee, J.-H.; Kim, S.-G.; Kim, M.-D. UV light driven high-performance room temperature surface acoustic wave NH₃ gas sensor using sulfur-doped g-C₃N₄ quantum dots. *Nano Res.* **2023**, 16, 7682–7695.
- (51) Zhu, M.; Ran, Q.; Huang, H.; Xie, Y.; Zhong, M.; Lu, G.; Bai, F.-Q.; Lang, X.-Y.; Jia, X.; Chao, D. Interface reversible electric field regulated by amphoteric charged protein-based coating toward high-rate and robust Zn anode. *Nano-Micro Lett.* **2022**, 14 (1), 219.
- (52) Hao, L.; Liu, Y.; Gao, W.; Han, Z.; Xue, Q.; Zeng, H.; Wu, Z.; Zhu, J.; Zhang, W. Electrical and photovoltaic characteristics of MoS₂/Si pn junctions. *J. Appl. Phys.* **2015**, 117 (11), 114502.
- (53) Xu, R. L.; Muñoz Rojo, M.; Islam, S.; Sood, A.; Vareskic, B.; Katre, A.; Mingo, N.; Goodson, K. E.; Xing, H. G.; Jena, D.; et al. Thermal conductivity of crystalline AlN and the influence of atomic-scale defects. *J. Appl. Phys.* **2019**, 126 (18), 185105.
- (54) Pasupuleti, K. S.; Chougule, S. S.; Vidyasagar, D.; Bak, N.-h.; Jung, N.; Kim, Y.-H.; Lee, J.-H.; Kim, S.-G.; Kim, M.-D. UV light driven high-performance room temperature surface acoustic wave NH₃ gas sensor using sulfur-doped g-C₃N₄ quantum dots. *Nano Res.* **2023**, 16 (5), 7682–7695.
- (55) Xu, X.; Zu, X.; Ao, D.; Yu, J.; Xiang, X.; Xie, W.; Tang, Y.; Li, S.; Fu, Y. NH₃-sensing mechanism using surface acoustic wave sensor with AlO (OH) film. *Nanomaterials* **2019**, 9 (12), 1732.
- (56) Li, X.; Li, X.; Li, Z.; Wang, J.; Zhang, J. WS₂ nanoflakes based selective ammonia sensors at room temperature. *Sens. Actuators, B* **2017**, 240, 273–277.
- (57) Liu, L.; Fei, T.; Guan, X.; Lin, X.; Zhao, H.; Zhang, T. Room temperature ammonia gas sensor based on ionic conductive biomass hydrogels. *Sens. Actuators, B* **2020**, 320, 128318.